Interventional real-time optical imaging guidance for complete tumor ablation

Xuefeng Kan[a,b], Feng Zhang[a], Guanhui Zhou[a,c], Hongxiu Ji[a], Wayne Monsky[a], Christopher Ingraham[a], Chuansheng Zheng[b], and Xiaoming Yang[a,1]

[a]Image-Guided Bio-Molecular Intervention Research and Division of Interventional Radiology, Department of Radiology, University of Washington School of Medicine, Seattle, WA 98109; [b]Department of Radiology, Union Hospital, Tongji Medical College, Huazhong University of Science and Technology, Wuhan 430022, China; and [c]Hepatobiliary and Pancreatic Interventional Treatment Center, Division of Hepatobiliary and Pancreatic Surgery, The First Affiliated Hospital, Zhejiang University School of Medicine, Hangzhou 310003, China

The aim of this study was to develop an interventional optical imaging (OI) technique for intraprocedural guidance of complete tumor ablation. Our study employed four strategies: 1) optimizing experimental protocol of various indocyanine green (ICG) concentrations/detection time windows for ICG-based OI of tumor cells (ICG cells); 2) using the optimized OI to evaluate ablation-heat effect on ICG cells; 3) building the interventional OI system and investigating its sensitivity for differentiating residual viable tumors from nonviable tumors; and 4) preclinically validating its technical feasibility for intraprocedural monitoring of radiofrequency ablations (RFAs) using animal models with orthotopic hepatic tumors. OI signal-to-background ratios (SBRs) among preablation tumors, residual, and ablated tumors were statistically compared and confirmed by subsequent pathology. The optimal dose and detection time window for ICG-based OI were 100 µg/mL at 24 h. Interventional OI displayed significantly higher fluorescence signals of viable ICG cells compared with nonviable ICG cells (189.3 ± 7.6 versus 63.7 ± 5.7 au, $P < 0.001$). The interventional OI could differentiate three definitive zones of tumor, tumor margin, and normal surrounding liver, demonstrating significantly higher average SBR of residual viable tumors compared to ablated nonviable tumors (2.54 ± 0.31 versus 0.57 ± 0.05, $P < 0.001$). The innovative interventional OI technique permitted operators to instantly detect residual tumors and thereby guide repeated RFAs, ensuring complete tumor eradication, which was confirmed by ex vivo OI and pathology. In conclusion, we present an interventional oncologic technique, which should revolutionize the current ablation technology, leading to a significant advancement in complete treatment of larger or irregular malignancies.

indocyanine green | interventional optical imaging | hepatic VX2 tumor | radiofrequency ablation | residual tumor

A dvances in image-guided percutaneous ablation technologies, such as radiofrequency ablation (RFA), microwave ablation, cryoablation, and irreversible electroporation, have greatly improved the management of malignancies in patients. These interventional oncologic therapies have some prominent advantages, including being minimally invasive and reproducible, offering low risk of complications and requiring only short hospital stay. However, with the current technology, these interventional ablation techniques are most effective at eradicating small (<3 cm) lesions (1, 2). For the ablation of larger and irregular lesions, these ablations appear to suffer the setback of incomplete tumor killing at the tumor periphery (3, 4). Residual viable tumor cells at the tumor periphery often serve as the source of tumor persistence and recurrence, ultimately leading to treatment failure (4–6).

Incomplete tumor ablation is attributed to the challenge of creating an effective and safe ablation periphery with a 1-cm surgical margin or "clear safety margin" beyond the tumor confinement using the current ablation technology (7, 8). The inability to obtain this clear margin is often caused by 1) infiltrative growth patterns of malignant tumors to form microsatellite lesions or microvenous

tumor emboli located at the 1-cm surgical margin of ablated tumors; 2) intentional avoidance of rapid overheating by the operator in order to protect adjacent critical structures (such as vasculatures, bile ducts, the gastrointestinal tract, and the diaphragm); 3) RFA heat carried away by blood flow when presence of larger neighboring vasculatures at the tumor periphery (so-called "heat-sink" effect); and 4) off-center positioning of the ablation electrode due to limited percutaneous access windows (9, 10).

For the clinical practice of percutaneous ablations, the primary reason for such incomplete tumor ablation is the current lack of an effective and real-time intraprocedural monitoring tool to instantly detect any residual tumor before terminating the ablation procedure. To date, the assessment of complete tumor treatment is either identified on postprocedure follow-up imaging or confirmed by postoperative pathology, if available.

Optical imaging (OI) represents the newest member of the modern medical imaging family. OI uses either near-infrared (NIR-I and NIR-II, 700 to 1,700 nm) or visible (400 to 700 nm) light to simultaneously provide molecular, morphologic, and functional information of disease processes (11). The primary advantages of OI include real-time imaging capability, cost-effectiveness, portability, nonionizing, and generally well-tolerated by patients (11, 12). Use of OI dyes [optical contrast agents, such as indocyanine green (ICG)] or advanced optical probes have further strengthened the usefulness of OI techniques in better detecting relatively deep-seated lesions and providing better strategies of guiding cancer treatments (13–15). These advancements in OI technology led to

Significance

We present an interventional optical imaging–guided oncologic technique. This interventional oncologic technique can differentiate, in vivo, the three definitive zones of tumor and tumor margin as well as normal surrounding liver, which enables differentiation of residual viable tumors from ablated nonviable tumors and thereby pretermit the intraprocedural real-time guidance for complete tumor eradication during a single interventional ablation session. This innovation should revolutionize the current ablation technology, leading to a significant advancement in the complete treatment of larger or irregular malignant lesions not only in the liver but also in other solid organs.

MEDICAL SCIENCES

www.manaraa.com

our current innovation, which specifically addresses the clinical problem of incomplete tumor ablation, by developing an interventional oncologic technique, named "Interventional real-time OI–guided complete tumor ablation" (Fig. 1).

Results

Study Design. This study consisted of four aims: 1) optimizing the ICG parameters, such as doses and detection time windows, specifically for in vitro experiments to achieve high-contrast and high-quality ICG-based OI of ICG-treated VX2 tumor cells (ICG cells); 2) using the optimized ICG-based OI to evaluate, in vitro, the ablation heat effect on ICG cells; 3) building an interventional real-time OI system with specific in vivo evaluation of its capability and sensitivity with accurate differentiation between the residual viable tumors and ablated nonviable tumors; and 4) via a preclinical longitudinal experiment using animal models with orthotopic liver VX2 tumors, to specifically validate the technical feasibility using the ICG-based interventional OI system to intraprocedurally guide complete tumor ablation, which closely mimicked image-guided percutaneous RFA of hepatic tumors in humans (Fig. 1).

Optimization of ICG Dose and Detection Time Window for In Vitro OI of ICG Cells. We first established the optimized protocol specifically for in vitro evaluation of ICG-based OI. VX2 tumor cells were treated with ICG at 1) different concentrations of 0, 25, 50, 75, 100, and 125 μg/mL for 24 h; 2) various incubation times of 1, 2, 4, 12, 24, and 48 h; and 3) nontreated cell groups served as a control. In optimization of ICG dose, fluorescent microscopy showed that intracellular uptake of ICG by VX2 cells was well established by emitting red fluorescence, which was not seen in VX2 cells without ICG treatment. The red fluorescence signals of these cells became more intense as we increased ICG concentrations from 0 to 125 μg/mL (Fig. 2A). In vitro quantitative optical/X-ray images of ICG cells further confirmed similar results to fluorescent microscopy, demonstrating that the fluorescence signal intensities (SIs) of ICG cells increased as ICG concentrations increased from 0 to the peak of 100 μg/mL and then remained constant. Thus, the optimum ICG dose for in vitro ICG-based OI was determined to be 100 μg/mL (Fig. 2 B and C).

When optimizing the timing for detection of ICG cells, fluorescent microscopy demonstrated that ICG-emitting red fluorescence became more intense as the incubation times increased from 0 to 48 h (Fig. 3A). In vitro optical/X-ray images of ICG cells showed similar results of increased fluorescence signals as the incubation duration was extended (Fig. 3B). The quantitative optical/X-ray imaging displayed ICG SI reached its peak at the incubation time point of 24 h, which thus was considered as the optimum detection time window for ICG-based in vitro OI of VX2 cells (Fig. 3C).

Ablation Heat Effect on ICG Cells. Once the optimized in vitro OI protocol was established, this was used to evaluate the ablation heat effect on ICG cells versus ICG solutions. After treating ICG cells by an ablation-mimicking lethal heat at 80 °C for 10 min, the immediate in vitro optical/X-ray image demonstrated a significant decrease in the average fluorescence SIs of ICG cells, compared with that before the ablation heat treatment ($4.13 \pm 0.26 \times 10^6$ photons/sec/mm^2 versus $13.65 \pm 0.56 \times 10^6$ photons/sec/mm^2, $P < 0.001$). However, no significant change of ICG fluorescence SIs was seen in the cells of the non–ablation-treated control groups ($13.23 \pm 0.99 \times 10^6$ photons/sec/mm^2 versus $13.25 \pm 0.80 \times 10^6$
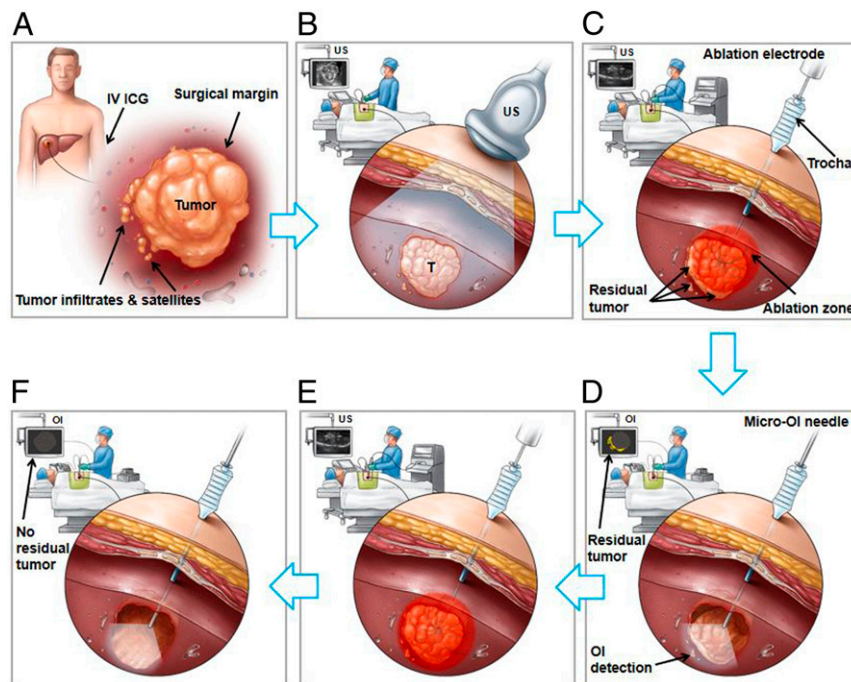

Fig. 1. Development of the interventional real-time OI-guided complete tumor ablation technique. (A) A tumor with an infiltrating border and microsatellite lesions at the 1-cm surgical margin. (B) Ultrasound imaging (US) allows for tumor visualization. (C) Real-time US-guided RFA. The incomplete tumor ablation leaves residual viable foci at the ablated tumor periphery. (D) Real-time use of the innovative interventional OI instantly detects residual tumor, which is specifically outlined by intravenous (IV) administration of the FDA-approved OI dye, ICG, depicted as optical signals (yellow color on the OI monitor screen) of the residual tumor at the ablation margin. The micro-optical needle is specifically designed to fit in any commercially available percutaneous interventional devices/instruments, such as an access trochar, and can be positioned via the same access trochar for placement of the percutaneous ablation electrode and then advanced into tumor to achieve intratumoral "inside-output" images along the ablated tumor margin. (E) Once residual tumor tissues are detected by the interventional OI, additional ablation with an adjusted larger ablation zone/energy or longer ablation time can be repeated until no ICG-outlined residual tumor is confirmed via the instant intraprocedural OI/repeat RFA approach during a single percutaneous ablation session (F).
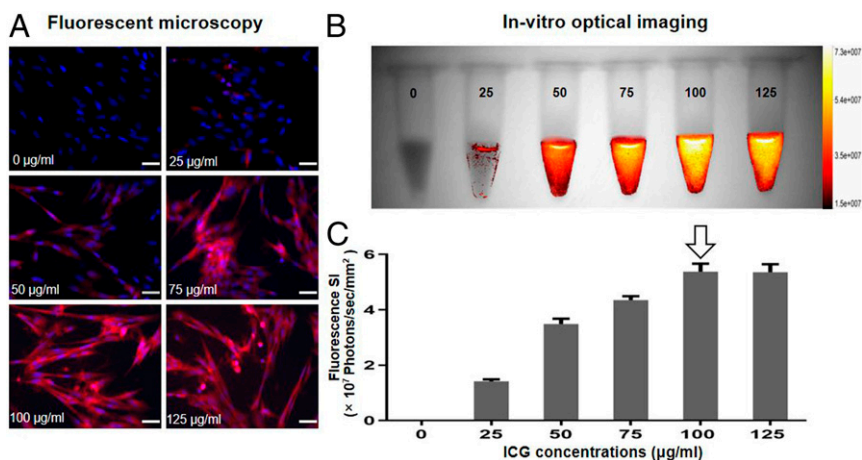
www.manaraa.com

Fig. 2. Optimization of ICG dose for in vitro OI of ICG-treated VX2 tumor cells (ICG cells). (*A*) Fluorescent microscopy images showed that the intracellular ICG fluorescence signal became more intense as ICG concentrations increased from 0 to 125 μg/mL. (*B*) The optical/X-ray images of ICG cells demonstrated an increase of fluorescence signal as ICG concentrations increased from 0 to 125 μg/mL. (C) Quantitative analysis of fluorescence SI further confirmed a similar SI between the concentrations of 100 and 125 μg/mL, which thus indicated the optimal concentration of 100 μg/mL (arrow) for ICG uptake by VX2 tumor cells. (Scale bars, 50 μm.)

photons/sec/mm^2, $P = 0.889$) (Fig. 4 *A* and *C*). After treating ICG solutions with the same ablation heat of 80 °C for 10 min, the immediate in vitro optical/X-ray images showed a significant decrease in the average fluorescence SIs of ICG solutions, compared with that before ablation heat treatment ($6.47 \pm 0.40 \times 10^7$ photons/sec/mm^2 versus $12.82 \pm 0.43 \times 10^7$ photons/sec/mm^2, $P < 0.001$). No significant change of the average fluorescence SIs was detected in the non–ablation-heated control groups ($12.66 \pm 0.50 \times 10^7$ photons/sec/mm^2 versus $12.69 \pm 0.52 \times 10^7$ photons/sec/mm^2, $P = 0.482$) (Fig. 4 *B* and *D*).

Fluorescent microscopy further demonstrated that the fluorescence signals of ICG cells was decreased, with smudged nuclei visualized after the ablation-heated treatment (Fig. 4 *E* and *F*). The findings were confirmed by the laboratory examinations with cell viability assay and flow cytometry analysis, showing no viable cells after the ablation heat treatment (Fig. 4 *G–I*). These results indicated that the ablation heat at 80 °C resulted in the destruction of ICG cells and depressed function of ICGs simultaneously.

Building the Interventional OI System. The interventional OI system was constructed by created a micro-OI needle of 30-cm length and

an outer diameter of 17 gauge. This type of micro-OI needle was specifically designed to be used in conjunction with any commercially available interventional devices/instruments, such as an access trochar used in image-guided percutaneous placement of ablation electrode. The OI needle was connected with 1) a 250-W halogen light source (KL 2500 LCD, Schott) that was equipped with a filter wheel containing an excitation filter (ET775/50x, Chroma Technology Corp.) and 2) a scientific complementary metal–oxide–semiconductor (sCMOS) camera (Pco.edge 4.2 bi; Pioneer in Cameras and Optoelectronics Aktien Gesellschaft) through a band pass emission filter (ET845/55m, Chroma Technology Corp.) (Fig. 5*A*).

In Vitro Interventional OI for Differentiation between Living (Viable) and Dead (Nonviable) ICG Cells. To evaluate the efficacy of interventional OI in differentiating the living ICG cells from the nonviable ICG cells, a cell phantom was created, consisting of a plastic tube that contained two separate chambers in the inferior portion (Fig. 5*C*). The living (viable) cells were centrifuged in one chamber with phosphate-buffered saline, while the dead (nonviable) tumor cells (treated by 80 °C of ablation heat) were present in the opposite chamber. The micro-OI needle was vertically positioned above the
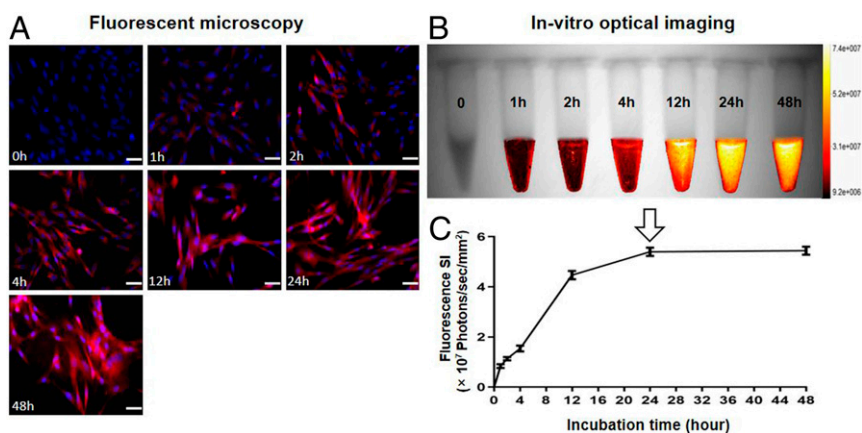

Fig. 3. Optimization of ICG time window for in vitro OI of ICG cells. (*A*) The fluorescent microscopy demonstrated that the intracellular ICG-emitting red fluorescence became more intense as the incubation time extended from 0 to 48 h. (*B*) The optical/X-ray images showed that the fluorescence signal of ICG cells reached its peak starting at a 24-h incubation time. (*C*) Quantitative analysis of the fluorescence SI further demonstrated the SI of ICG cells increased during the 0- to 24-h incubations and then plateaued until the 48-h time point, which thus confirmed the optimal time window for ICG-based in vitro OI to be 24 h (arrow) post-ICG uptake by VX2 tumor cells. (Scale bars, 50 μm.)
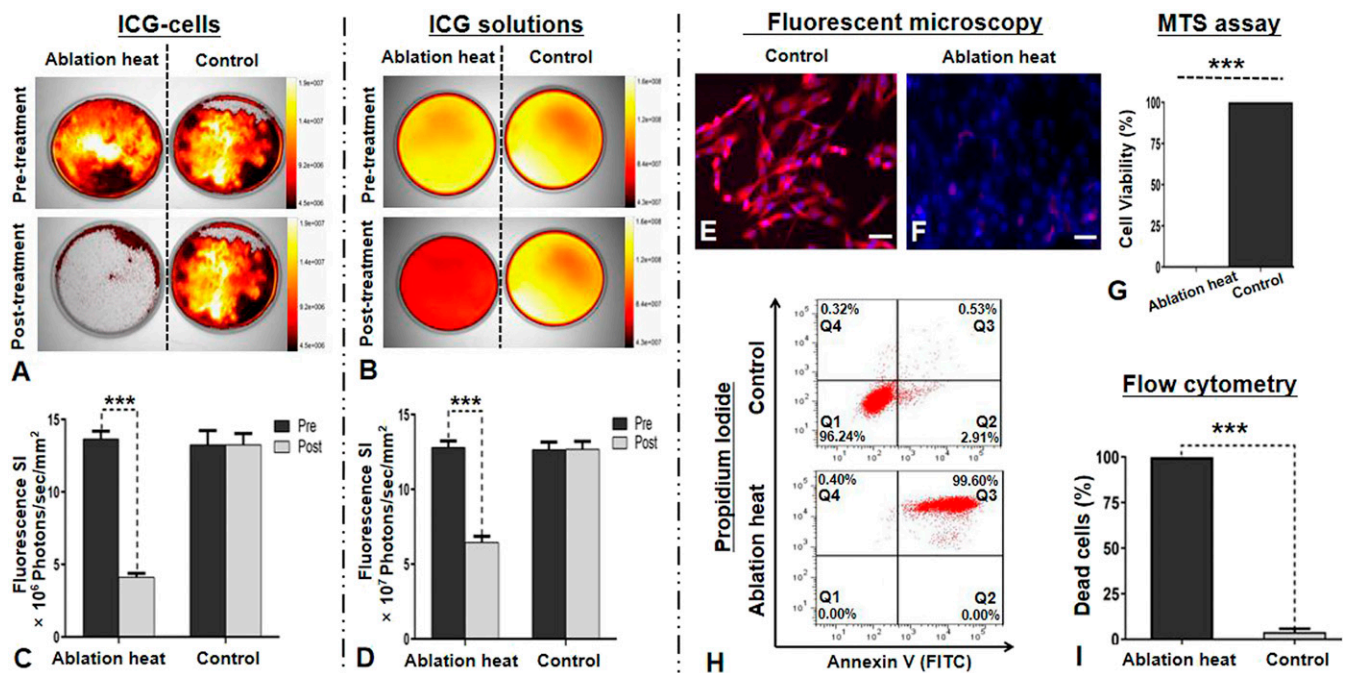
Kan et al.
Interventional real-time optical imaging guidance for complete tumor ablation

Fig. 4. In vitro OI for the evaluation of ablation heat effect on ICG-treated VX2 tumor cells (ICG cells) and ICG solutions. (*A* and *B*) The optical/X-ray images demonstrated clearly the decreased fluorescence signals (yellow-orange) of both ICG cells and ICG solutions after the lethal ablation heat treatment at 80 °C, while no signal changes were noted in the non–ablation-heat control groups. (*C* and *D*) Quantitative analysis further confirmed a significant decrease in the fluorescence SIs of the ablation-heated ICG cells and ICG solutions, with no significant SI changes in the controlled ICG cells and ICG solutions. (*E* and *F*) Fluorescent microscopy images further displayed that fluorescence signals of ICG cells were clearly decreased with smudged nuclei after the ablation heat treatment, compared with the non–ablation-heated control cells. (*G*) The MTS (3-(4,5-dimethylthiazol-2-yl)-5-(3-carboxymethoxyphenyl)-2-(4-sulfophenyl)-2H-tetrazolium) assay showed no viable cells after the ablation heat treatment. (*H* and *I*) Flow cytometry further confirmed almost 100% nonviable cells (red in Q3 zone) after the ablation heat treatment, compared with the viable cells (red in Q1 zone) of the control group without ablation heat treatment. (Scale bars, 50 μm.) A paired Student's *t* test was used for statistical analysis (***$P < 0.001$).

two cell-containing chambers to generate in vitro interventional OI (Fig. 5 *B–D*).

Interventional OI clearly detected the high fluorescence signals emitted from the living ICG cells, in sharp contrast to the low fluorescence signals from the dead ICG cells (Fig. 6*D*), which was later confirmed by fluorescent microscopy displaying as the decreased ICG signals of cells with smudged nuclei after the ablation heat treatment (Fig. 5 *E* and *F*). The quantitative analysis of fluorescence SIs further confirmed a significantly higher average fluorescence SI of the living ICG cells, in comparison with the ablation-treated nonviable ICG cells (189.3 ± 7.6 au versus 63.7 ± 5.7 au, $P < 0.001$) (Fig. 5*G*).

Creation of VX2 Tumor Models. The primary goal for the in vivo experiments was to evaluate the functionality/sensitivity of the interventional OI system, which was required in conjunction with commercially available percutaneous interventional devices/instruments. For this objective, the use of larger animal models was ideal. To date, the preexisting rabbit model employing VX2 liver tumors has been the most well-accepted model for basic/preclinical research in hepato-oncology (16–18). Thus, in this study, we created 24 rabbit models with orthotopic hepatic VX2 tumors (Fig. 6).

In Vivo Real-Time Interventional OI of Liver Tumors. With the interventional OI system, three distinct histopathologic zones, including tumor, tumor margin, and the surrounding normal liver (background fluorescence), could be clearly visualized in vivo. This could only be seen ex vivo using traditional pathology examination of either surgically removed or biopsied and autopsied tumor tissues if available (Fig. 7).

Capability and Sensitivity Using the Interventional OI in Differentiating Residual Viable Tumors from Ablated Nonviable Tumors. Under real-time ultrasound imaging guidance, a multipolar RFA electrode, connected to an RFA generator (WE7568-II, Welfare Electronics Co.), was positioned into the tumor center during RFA treatment. To evaluate the capability/sensitivity of the interventional OI system, 16 animals with RFA-treated tumors were divided into two tumor model groups (8 per group): 1) incomplete ablation was achieved by not fully deploying the prongs of the multipolar RFA electrode which intentionally destroyed only part of the tumor, leaving a viable portion of the tumor along the tumor margin and 2) complete ablation to include the tumor margin by fully deploying the prongs of the RFA electrode to completely destroy the tumor. The partial or complete deployment of the electrode prongs to include the target tumor margins was precisely guided by real-time ultrasound imaging and later confirmed by X-ray imaging (Fig. 8 *A–C*, *F*, and *G*). All tumors were ablated at a lethal heat temperature of 80 °C for 4 min.

The interventional OI of the incompletely ablated tumor group was detected by the high fluorescence signals present in both the residual tumors and preablation tumors. However, low signals were detected in the ablated tumors. These findings were further confirmed by quantitative SI analysis with significantly higher average signal-to-background ratios (SBRs) in the peripheral residual tumors and preablation tumors (residual tumors versus ablated tumors = 2.54 ± 0.31 versus 0.57 ± 0.05, $P < 0.001$; preablation tumors versus ablated tumors = 2.52 ± 0.42 versus 0.57 ± 0.05, $P < 0.001$) (Fig. 8 *D*, *E*, and *K*). No statistically significant difference in the average SBRs were detected between the preablation tumors and residual tumors (2.52 ± 0.42 versus 2.54 ± 0.31, $P = 0.751$). The interventional OI of the completely ablated tumor group was detected as high signals in the preablation tumor, with a significantly
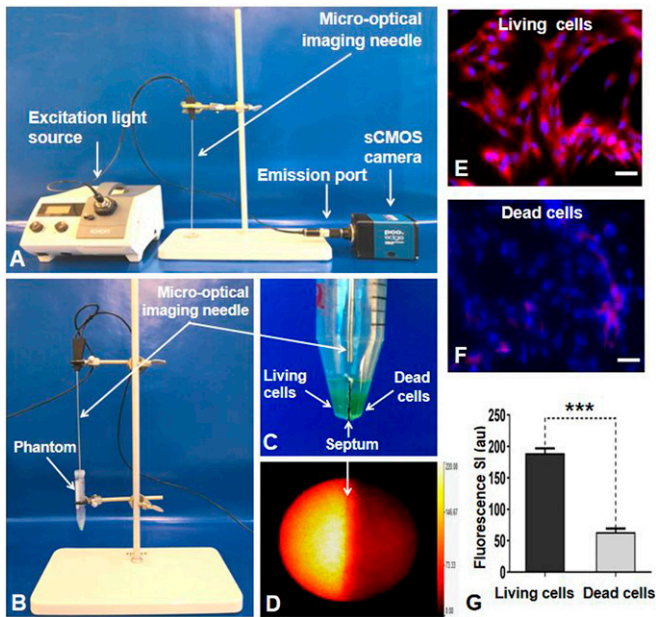
www.manaraa.com

Fig. 5. (*A*) The interventional OI system. Because of the designed needle type, the micro-OI needle could be inserted to the tumor via a percutaneous access to achieve an "inside-output" real-time intratumoral imaging. (*B* and *C*) In vitro experimental setup for evaluating the interventional OI system. A cell phantom was created, consisting of a plastic tube that had two separate chambers in the inferior portion (*C*). The living (viable) tumor cells were centrifuged in one chamber, with nonviable tumor cells (treated by 80 °C heat) in the opposite chamber. The micro-OI needle was vertically positioned in the phantom, just above the two cell-containing chambers. (*D*) Real-time interventional optical image, demonstrating a high ICG signal (yellow) for the living cell group compared with the dead cell group, which was further confirmed by fluorescent microscopy (*E* and *F*) and fluorescent SI quantification (*G*). (Scale bars, 50 μm.) A paired Student's *t* test was used for statistical analysis (***$P < 0.001$).

reduced signal in the completely ablated tumor. A significantly higher average SBR was present in the preablation tumor group compared with that of the postablated tumor group (2.54 ± 0.34 versus 0.57 ± 0.04, $P < 0.001$) (Fig. 8 *I*, *J*, and *L*).

Confirmation with Ex Vivo OI. The ex vivo OI of the gross, sectioned specimen functions as a "Gold standard" to corroborate the findings achieved by the in vivo interventional OI system, with final confirmation by pathologic examination. As shown in Fig. 9, ex vivo OI further confirmed the findings by in vivo interventional OI, demonstrating that the average SBR of the completely ablated tumors was significantly lower than that of the normal liver (0.58 ± 0.04 versus 1.00 ± 0.00, $P < 0.001$), and the average SBR of the residual

tumors was significantly higher than that of the normal liver and the ablated tumor (residual tumors versus normal liver = 2.56 ± 0.39 versus 1.00 ± 0.00, $P < 0.001$; residual tumors versus ablated tumors = 2.56 ± 0.39 versus 0.58 ± 0.03, $P < 0.001$).

The in vivo and ex vivo OI findings in the sections *Capability and Sensitivity Using the Interventional OI in Differentiating Residual Viable Tumors from Ablated Nonviable Tumors* and *Confirmation with Ex Vivo OI* were further confirmed by pathologic examination with hematoxylin and eosin (H&E) staining, terminal deoxynucleotidyl transferase dUTP nick end labeling staining, Ki67 staining, and fluorescent microscopy (Fig. 10).

Preclinical Longitudinal Validation of the Technical Feasibility. We further validated the technical feasibility of the ICG-based interventional OI technique via serial in vivo experiments to assist intraprocedurally in achieving complete tumor ablation at a longitudinal and more-preclinical setting by closely mimicking image-guided percutaneous RFA of hepatic tumors in humans (Fig. 1). When incomplete ablation, the interventional OI could clearly identify the high fluorescence signals being emitted from the residual tumor compared with the low signals emitted in the ablated tumor. The average SBRs of the residual tumor and preablation tumor were significantly higher than that of the ablated tumor (residual tumors versus ablated tumors = 2.56 ± 0.10 versus 0.58 ± 0.03, $P < 0.001$; preablation tumors versus ablated tumors = 2.52 ± 0.14 versus 0.58 ± 0.03, $P < 0.001$), and there was no statistically significant difference of the average SBRs between the preablation tumor and residual tumor (2.52 ± 0.14 versus 2.56 ± 0.10, $P = 0.219$). After a complete ablation, the interventional real-time OI detected low fluorescence signal in the fully ablated tumor. The average SBR of an ablated tumor was significantly lower than that of the normal liver (0.57 ± 0.02 versus 1.00 ± 0.00, $P < 0.001$) and the preablation tumor (0.57 ± 0.02 versus 2.52 ± 0.14, $P < 0.001$). The ex vivo OI, H&E staining, and fluorescent microscopy further confirmed that the tumor was completely ablated (Fig. 11).

Discussion

Residual viable tumor cells that located at the periphery of larger or irregular malignancies are frequently responsible for residual disease and/or recurrence using current interventional ablation technologies. In clinical practice, the primary reason for such incomplete tumor ablation is the absence of an intraprocedural real-time imaging tool, which would allow for residual tumors to be instantly detected before terminating the ablation procedure. In current clinical practice, residual tumor is usually identified on postablation follow up imaging, such as computed tomography (CT), positron emission tomography/computed tomography (PET/CT), and MRI. However, these follow-up imaging modalities often detect persistent or recurrent tumor at days/weeks to months after terminating the initial ablation (19–21). Thus, it is imperative to
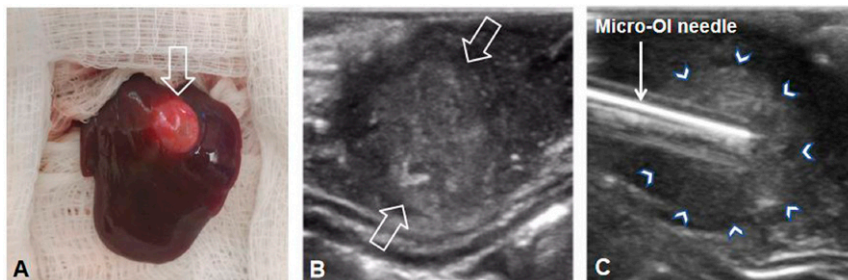

Fig. 6. Creation of the rabbit model with VX2 liver tumor. (*A*) A VX2 liver tumor (open arrow) was successfully created in the left lobe of the rabbit liver, which was detected by ultrasound imaging (between open arrows in *B*). Under real-time ultrasound imaging guidance, the micro-OI needle could be advanced into the tumor and then precisely positioned at different directions along the tumor margin (arrowheads in *C*) to detect ICG-outlined residual tumors.
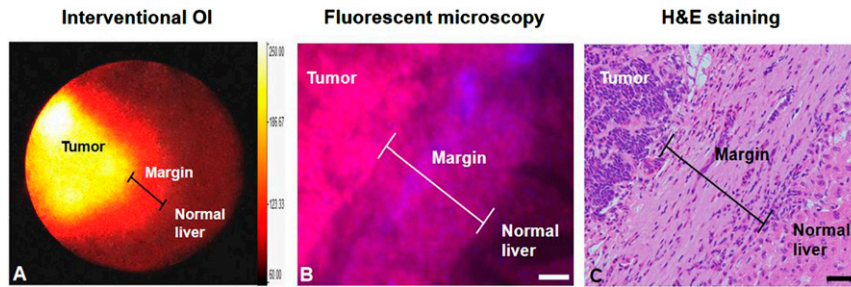
Kan et al.
Interventional real-time optical imaging guidance for complete tumor ablation

PNAS | 5 of 9
https://doi.org/10.1073/pnas.2113028118

www.manaraa.com

Fig. 7. (*A*) In vivo interventional OI clearly demonstrates the three definite zones: tumor, tumor margin, and surrounding normal liver. These can only be seen, ex vivo, by traditional pathology examination of tumor tissues from either surgical removal or biopsied and autopsied tumor tissues (*B* and *C*). (Scale bars, 50 μm.)

develop a new intraprocedural real-time imaging tool, allowing immediate detection of residual tumors at the ablated tumor periphery during a single ablation session. The innovative design of the present study aims to specifically conquer the critical clinical problem of residual or recurrent tumor following RFA of larger and irregular malignancies: developing a "one-stop-shop" interventional oncologic technology "Intraprocedural real-time OI guidance for complete tumor ablation," with a specific emphasis on the full eradication of malignant cells located at the difficult to treat tumor periphery, to create clean tumor (surgical) margins.

OI has several important advantages over other imaging modalities, such as CT or PET/CT (with no real-time imaging capability) and MRI (with high cost and environment requirements for MR safety). Recent advances in OI using target optical probes have further enhanced the ability of OI to detect deeper lesions and allow for better planning and guidance of localized cancer treatments (13–15). However, these novel OI compounds are still in preclinical development phase and a long way from regulatory

approval (22). Thus, considering the potential smooth translation of the interventional OI technique to a further clinical trial, in this study we specifically selected the Food and Drug Administration (FDA)-approved fluorescent agent, ICG, as the OI contrast agent, with our goal being to achieve superior imaging quality for instant detection of residual foci at the ablated tumor periphery during the ablation procedure.

ICG is an intracellular and relatively nontoxic protein-bound compound (13, 23). The potential mechanisms for intracellular localization of ICG have not been fully understood yet. A few studies suggest that the hepatic malignant tumor cells can take up ICG via the transporters of Na^+/taurocholate cotransporting polypeptide and organic anion transporting polypeptide 8 (24). Intravenously administered ICG is excreted exclusively by the normal bile duct of liver. However, as the impaired biliary excretion in the cancer tissues, ICG is accumulated in the liver tumor cells, which thus results in ICG enhancement throughout the tumor, and thereby ICG-outlined tumors can be detected by OI.
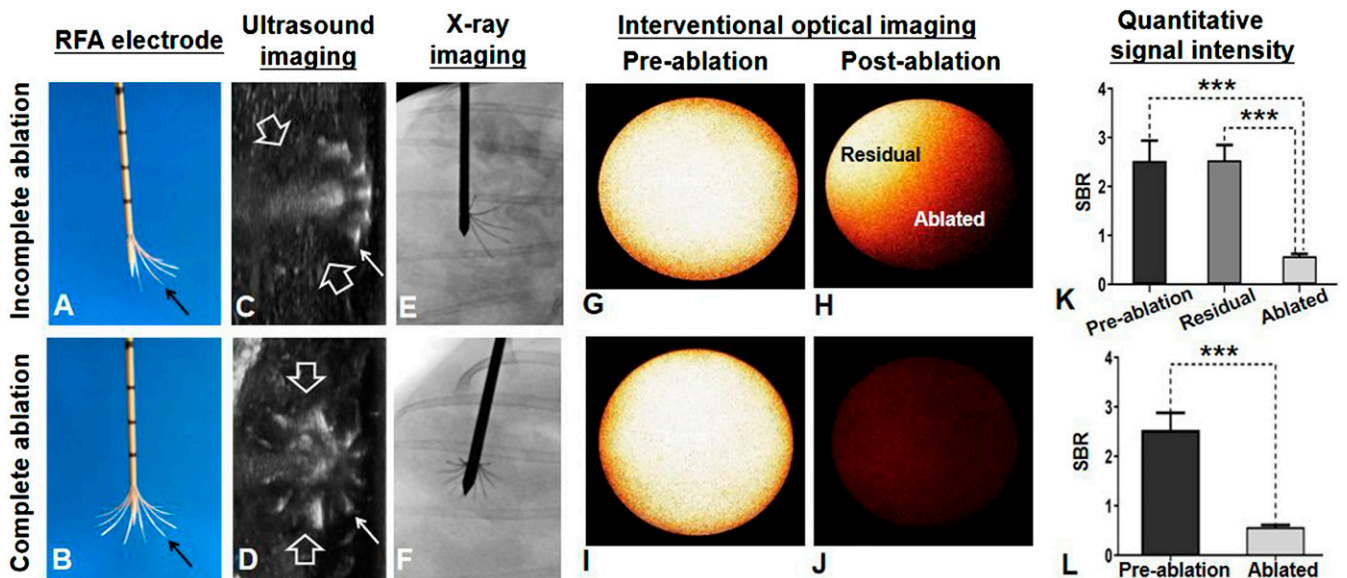

Fig. 8. (*A* and *B*) RFA electrodes with (*A*) incomplete opening of the prongs (arrow), which allowed for creation of the tumor model with residual tumor at the unablated portion of the tumor margin and (*B*) complete opening of the entire prongs to fully cover the entire tumor margin for complete tumor ablation. (*C* and *D*) Axial ultrasound images, showing the placement of RFA electrodes in the tumors (between open arrows), with partial opening (*C*) or full opening (*D*) of electrode prongs (small arrows), which were precisely monitored and controlled under ultrasound imaging guidance and confirmed by X-ray imaging (*E* and *F*). (*G*, *H*, *I*, and *J*) In vivo ICG-based interventional OI of incomplete tumor ablation, showing residual tumor as high signal (yellow on *H*) and ablated portion of the tumor as low signal (*H*), while no signal was detected after complete ablation of the tumor (*J*), in comparison with preablation of the tumors with high signal (*G* and *I*). (*K* and *L*) These OI findings were further confirmed by quantitative analysis of SBR, demonstrating significant lower average SBR of ablated tumors, in comparison with those preablation tumors and residual tumors. A paired Student's t test was used for statistical analysis (***$P < 0.001$).
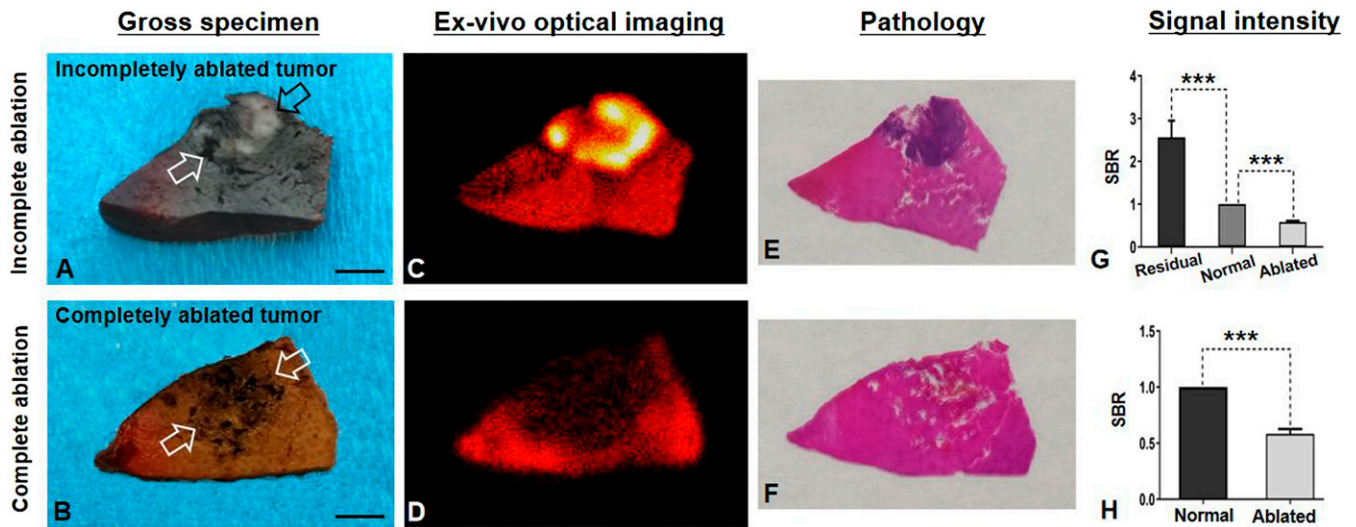
www.manaraa.com

Fig. 9. Ex vivo OI of gross specimens of incompletely versus completely ablated tumors (open arrows in *A* and *B*). The incompletely ablated residual tumor tissues appeared as white (open arrows in *A*), which was clearly outlined by ICG-based OI (yellow in *C*), compared with the completely ablated tumor in *B* and *D*. (*E* and *F*) OI findings were confirmed by pathology, demonstrating the residual tumor tissues as a blue color with H&E staining (*E*), which was not seen in the completely ablated tumor (*F*). (*G* and *H*) Quantitative analysis further confirmed significant higher average signal-to-background ratio (SBR) in residual tumors than those of surrounding normal liver tissue and the ablated tumor, while the average SBR of completely ablated tumors was significantly lower than that of the surrounding normal liver. (Scale bars, 1 cm.) A paired Student's *t* test was used for statistical analysis (***$P < 0.001$).

ICG has been used for management of different cancers (25–27). In open liver surgery for example, the operators use an external ICG-based OI imager to obtain surface fluorescence images for the planning of liver tumor resection (24, 28). However, the surface OI for the detection of deep-seated small lesions has been a challenging task, since the tissue penetration depth of current ICG-based fluorescence imaging is ~1 cm (24, 29). This problem, the limited penetration depth of current OI, can be solved using image-guided interventional approaches, which are capable of precisely

guiding the position of micro-OI detectors to the targets, avoiding tissue scattering and reflection along the pathway of OI light.

In the present study, we attempted to fully apply the advantages of ICG-based OI by extending its use from open surgeries to image-guided, minimally invasive interventional oncology treatment for the thermal ablation of hepatic tumors as the first target. Under real-time image guidance, deep-seated tumors were accurately localized, allowing for the interventional micro-OI needle to be precisely positioned into the tumors. As the tumors were
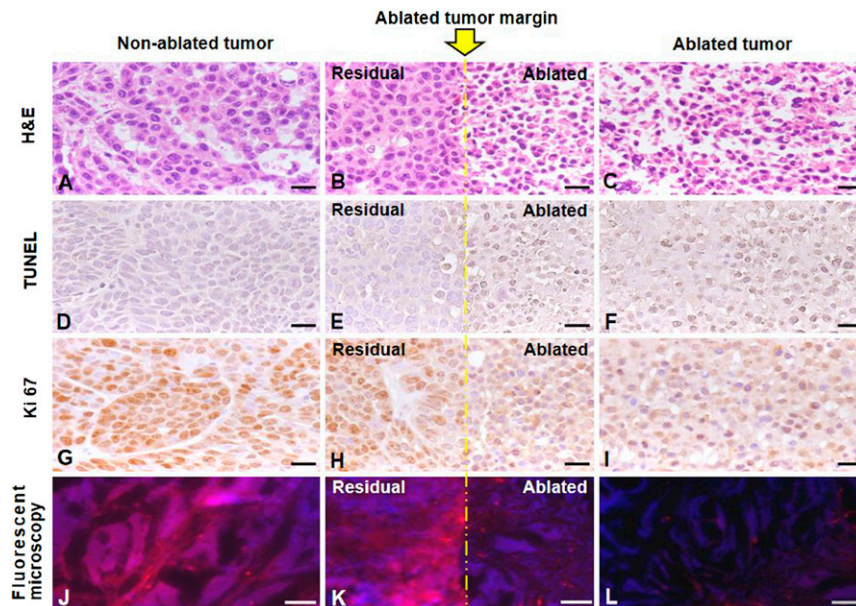

Fig. 10. Pathology results with different staining. Yellow line indicates the ablated tumor margin. (*A–C*) H&E staining confirmed tumor formation (*A*), as well as the smudged cellular nucleus (*C*) after the lethal ablation. (*D–F*) Terminal deoxynucleotidyl transferase dUTP nick end labeling (TUNEL) staining demonstrated more dead cells (brown in *E* and *F*) in the ablated tumor. (*G–I*) Ki67 staining showed more cell proliferation (brown in *G* and *H*) in the residual (*H*) and the nonablated tumor (*G*). (*J–L*) Fluorescent microscopy more clearly demonstrated the residual and viable tumor cells (pink in *J* and *K*), as outlined by ICG, which further confirmed the sensitivity of ICG-based OI developed in this study, for differentiating the surviving (viable) tumors from dead (nonviable) tumors during an ablation procedure. [Scale bars (H&E, TUNEL, and Ki67), 20 μm; scale bar (Fluorescent microscopy), 50 μm.]
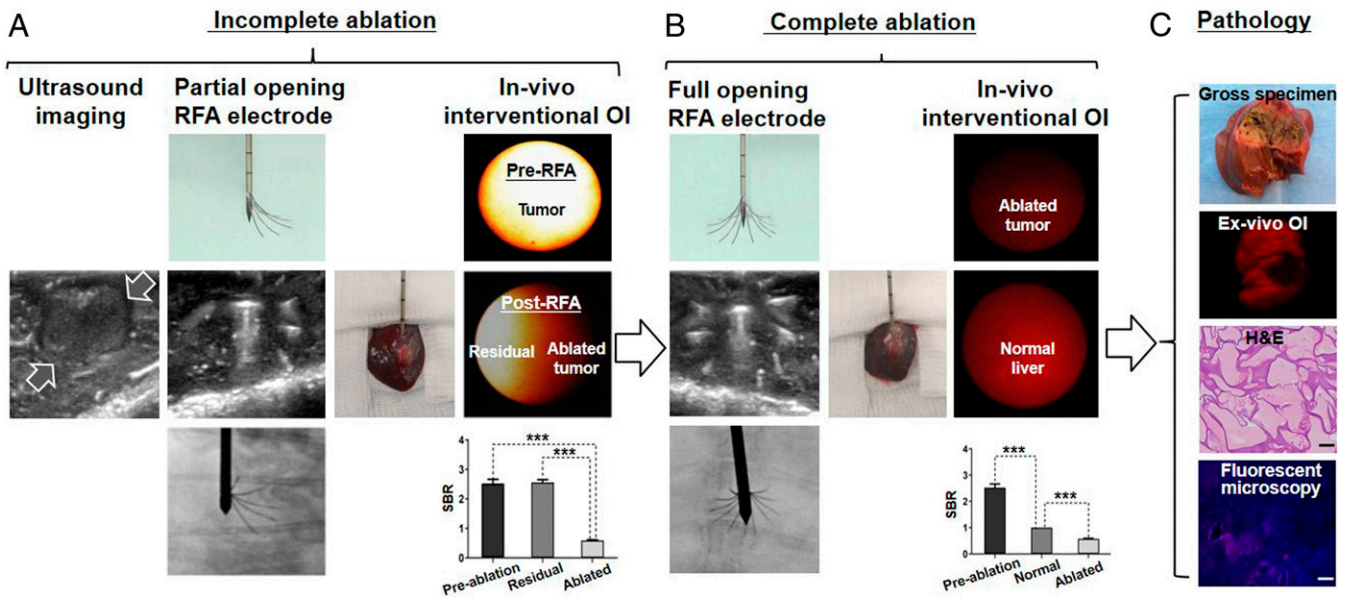
Fig. 11. Preclinical longitudinal validation of the technical feasibility of the interventional OI. (*A*) Ultrasound imaging detected the tumor (between open arrows). An incompletely ablated tumor was purposely created, and the interventional OI with quantifying SBR analysis was used to instantly detect the residual tumor, which demonstrated high fluorescence signals (yellow). (*B*) Based on findings of the interventional OI, the ablation was repeated with a larger ablation zone and increased energy to specifically destruct the residual tumor. Thus, the intraprocedural real-time OI guidance ensured the final complete tumor ablation, which demonstrated a low fluorescence signal in the ablated tumor. (*C*) Ex vivo OI and subsequent pathology with different examinations finally confirmed complete tumor eradication (necrosis). [Scale bar (H&E), 20 μm; scale bar (fluorescent microscope), 50 μm.] A paired Student's *t* test was used for statistical analysis (***$P < 0.001$).

ablated, interventional OI was generated, and residual viable foci at the ablated tumor periphery could then be detected. With this strategy, we specifically designed and built the interventional OI system, which was equipped with a micro-OI needle, ICG-specific excitation and emission filters, and a high-performance digital sCMOS camera, to acquire the intratumoral near-infrared fluorescence signals emitting from ICG-outlined tumors. The interventional OI technique enables intraprocedural identification of residual viable foci of ablated tumors. This information provides immediate feedback to the interventionalists performing the procedure to carry out further action by either extending the ablation duration, increasing the ablation zone/energy, or repositioning the ablation electrode to assure the complete eradication of the entire tumor during an image-guided percutaneous ablation session.

Through the serial comprehensive in vitro experiments with VX2 tumor cells, we first need to optimize the in vitro experimental protocol of ICG dose and detection time window to achieve a satisfactory ICG based OI. By applying the optimum in vitro OI protocol, we confirmed the hypothesis that the micro-optical needle–based interventional OI apparatus could sensitively differentiate the living (viable) tumor cells from the ablated dead (nonviable) tumor cells. Subsequently, through serial in vivo experiments using larger animal (rabbit) models with orthotopic liver VX2 tumors, we further investigated the capability and sensitivity of this novel interventional OI system in identifying the residual foci of the ablated tumors. Ex vivo OI, as well as different pathology and laboratory examinations served as "gold standards" for comparison with the interventional OI system. In the final step of this study, we successfully validated the technical feasibility of the interventional OI system in a more-realistic clinical setting by mimicking the image-guided tumor ablation process in humans using the interventional OI for real-time guidance during the ablation process to differentiate incomplete and complete RFA. Thus, these comprehensive in vitro, ex vivo, and in vivo experiments in this study have allowed for the establishment of the interventional oncology technique. The intraprocedural OI/RFA protocol, as exemplified and optimized by

this study, has demonstrated the essential aspects of this technique and will facilitate its eventual translation to clinical practice.

In conclusion, we present an innovative interventional oncologic technique: "Interventional real-time OI guidance for complete tumor ablation." This technique and approach may revolutionize current ablation technology by changing real-time imaging capabilities and decision making during an image-guided intervention ablation session. This could lead to a significant advancement in the complete eradication of larger and irregular malignant lesions, not only in the liver but also in other solid organs. This will, in turn, greatly improve survival and the quality of life in patients suffering from unresectable solid organ malignancies.

Materials and Methods

Details of in vitro, in vivo, and ex vivo OI experiments are described in *SI Appendix, Materials and Methods*.

Cell Culture. VX2 tumor cells were cultured under different conditions for various examinations and evaluations, including 1) 1×10^5 cells seeded in 35×10-mm Petri dishes (Falcon, Becton Dickinson and Company) for in vitro optical/X-ray imaging, 2) 5×10^4 cells per chamber seeded in four-well chamber slides (Lab-TekII; Thermo Fisher Scientific) for fluorescent microscopy confirmation, and 3) 5×10^5 cells seeded in 100×20–mm Petri dishes (Falcon, Corning Incorporated) for interventional OI. All VX2 tumor cells were cultured by Roswell Park Memorial Institute medium 1640 (Gibco, Paisley, PA4 9RF) supplemented with 10% fetal bovine serum (Gibco) and incubated at 37 °C with a 5% carbon dioxide atmosphere. When 80% confluence was reached, cells were treated with ICG (Patheon Italia S.P.A) at different concentrations and various incubation times and then examined using optical/X-ray imaging, fluorescent microscopy, and interventional OI.

In-Vivo Interventional Real-Time OI. Twenty-four hours before RFA procedures, all animals received intravenous administration of ICG via an auricular vein (0.5 mg/kg body weight) (30). Before and after RFA, under ultrasound imaging guidance, the micro-OI needle was first positioned in the normal liver parenchyma just outside of the RFA electrode entering the tumor to achieve background interventional OI. Then, under real-time ultrasound imaging guidance, the micro-OI needle was advanced to the tumor periphery and achieved intratumoral "inside-output" OI at six different directions/points around the tumor

www.manaraa.com

periphery (i.e., at 3, 6, 9, and 12 o'clock along the equator as well as the north and south poles) using the same interventional OI protocol as used for in vitro interventional OI in the section pertaining to in-vitro interventional OI of ICG-cells with and without ablation-heated treatments.

Ex-Vivo OI Confirmation. Briefly, after achieving satisfactory in vivo interventional OI, the rabbits were euthanized, and the left liver lobe with the tumor was harvested and sliced at the thickness of 0.5 to 0.8 cm. These gross liver specimens were then imaged using the Bruker In Vivo Xtreme optical/X-ray imaging system at the excitation wavelength of 760 nm, emission wavelength of 830 nm, field of view of 120 × 120 mm, 1.40 F-Stop, 2 × 2 binning, and an exposure time of 1.0 min.

Statistical Analysis. Three investigators independently interpreted the results from the in vitro, ex vivo, and in vivo experiments in each of the study sections. The statistical analysis with a paired Student's t test was performed using the Statistical Product and Service Solutions 24.0 software (IBM). The average fluorescence SIs and the average SBRs were compared with the different subject groups undergoing the different treatments. Data were expressed as mean $\pm$ SD. A probability level of less than 0.05 was considered statistically significant.

Data Availability. All data used for the study are within the manuscript and *SI Appendix*.

1. A. Facciorusso, G. Serviddio, N. Muscatiello, Local ablative treatments for hepatocellular carcinoma: An updated review. *World J. Gastrointest. Pharmacol. Ther.* **7**, 477–489 (2016).
2. R. M. Eisele *et al.*, Results of liver resection in combination with radiofrequency ablation for hepatic malignancies. *Eur. J. Surg. Oncol.* **36**, 269–274 (2010).
3. J. P. McWilliams *et al.*, Percutaneous ablation of hepatocellular carcinoma: Current status. *J. Vasc. Interv. Radiol.* **21**, S204–S213 (2010).
4. B. M. Künzli, P. Abitabile, C. A. Maurer, Radiofrequency ablation of liver tumors: Actual limitations and potential solutions in the future. *World J. Hepatol.* **3**, 8–14 (2011).
5. J. E. Hwang *et al.*, Combination of percutaneous radiofrequency ablation and systemic chemotherapy are effective treatment modalities for metachronous liver metastases from gastric cancer. *Clin. Exp. Metastasis* **31**, 25–32 (2014).
6. R. Iezzi *et al.*; HepatoCATT Group for the Multidisciplinary Management of HCC, Single-step multimodal locoregional treatment for unresectable hepatocellular carcinoma: Balloon-occluded percutaneous radiofrequency thermal ablation (BO-RFA) plus transcatheter arterial chemoembolization (TACE). *Radiol. Med. (Torino)* **118**, 555–569 (2013).
7. M. D. Beland, E. J. Wasser, W. W. Mayo-Smith, D. E. Dupuy, Primary non-small cell lung cancer: Review of frequency, location, and time of recurrence after radiofrequency ablation. *Radiology* **254**, 301–307 (2010).
8. M. Ahmed *et al.*; International Working Group on Image-Guided Tumor Ablation; Interventional Oncology Sans Frontières Expert Panel; Technology Assessment Committee of the Society of Interventional Radiology; Standard of Practice Committee of the Cardiovascular and Interventional Radiological Society of Europe, Image-guided tumor ablation: Standardization of terminology and reporting criteria–A 10-year update. *J. Vasc. Interv. Radiol.* **25**, 1691–705.e4 (2014).
9. A. A. van Tilborg *et al.*, MWA versus RFA for perivascular and peribiliary CRLM: A retrospective patient- and lesion-based analysis of two historical cohorts. *Cardiovasc. Intervent. Radiol.* **39**, 1438–1446 (2016).
10. S. Bhatia *et al.*, Radiofrequency ablation in primary non-small cell lung cancer: What a radiologist needs to know. *Indian J. Radiol. Imaging* **26**, 81–91 (2016).
11. G. Di Leo, R. M. Trimboli, T. Sella, F. Sardanelli, Optical imaging of the breast: Basic principles and clinical applications. *AJR Am. J. Roentgenol.* **209**, 230–238 (2017).
12. P. Causin, M. G. Lupieri, G. Naldi, R. M. Weishaeupl, Mathematical and numerical challenges in optical screening of female breast. *Int. J. Numer. Methods Biomed. Eng.* **36**, e3286 (2019).
13. A. Pansa, G. Torzilli, F. Procopio, D. Del Fabbro, Indocyanine-green fluorescence guided anatomical segmentectomy for HCC with portal thrombosis: The counter-fluorescence technique. *Updates Surg.* **72**, 219–222 (2020).
14. M. B. Reinhart, C. R. Huntington, L. J. Blair, B. T. Heniford, V. A. Augenstein, Indocyanine green: Historical context, current applications, and future considerations. *Surg. Innov.* **23**, 166–175 (2016).
15. H. Nishino *et al.*, Real-time navigation for liver surgery using projection mapping with indocyanine green fluorescence: Development of the novel medical imaging projection system. *Ann. Surg.* **267**, 1134–1140 (2018).
16. X. Kan *et al.*, Stress test of contrast-enhanced US with phenylephrine in a rabbit VX2 liver tumor model: Differentiating benign periablational enhancement from residual tumor after radiofrequency ablation. *J. Vasc. Interv. Radiol.* **27**, 1077–1085.e2 (2016).
17. J. M. M. van Breugel *et al.*, Theranostic application of lipiodol for transarterial chemoembolization in a VX2 rabbit liver tumor model. *Theranostics* **9**, 3674–3686 (2019).
18. R. Duran *et al.*, Vandetanib-eluting radiopaque beads: Pharmacokinetics, safety, and efficacy in a rabbit model of liver cancer. *Radiology* **293**, 695–703 (2019).
19. S. K. Kim *et al.*, Hepatocellular carcinoma treated with radio-frequency ablation: Spectrum of imaging findings. *Radiographics* **23**, 107–121 (2003).
20. X. Kan *et al.*, Combined ultrasound/computed tomography guidance in percutaneous radiofrequency ablation after transarterial chemoembolization for hepatocellular carcinoma in the hepatic dome. *Cancer Manag. Res.* **11**, 7751–7757 (2019).
21. X. Y. Wang, D. Chen, X. S. Zhang, Z. F. Chen, A. B. Hu, Value of ^{18}F-FDG-PET/CT in the detection of recurrent hepatocellular carcinoma after hepatectomy or radiofrequency ablation: A comparative study with contrast-enhanced ultrasound. *J. Dig. Dis.* **14**, 433–438 (2013).
22. S. Kurbegovic *et al.*, Molecular targeted NIR-II probe for image-guided brain tumor surgery. *Bioconjug. Chem.* **29**, 3833–3840 (2018).
23. J. A. Carr *et al.*, Shortwave infrared fluorescence imaging with the clinically approved near-infrared dye indocyanine green. *Proc. Natl. Acad. Sci. U.S.A.* **115**, 4465–4470 (2018).
24. T. Ishizawa *et al.*, Mechanistic background and clinical applications of indocyanine green fluorescence imaging of hepatocellular carcinoma. *Ann. Surg. Oncol.* **21**, 440–448 (2014).
25. T. Kokudo *et al.*, Assessment of preoperative liver function for surgical decision making in patients with hepatocellular carcinoma. *Liver Cancer* **8**, 447–456 (2019).
26. C. K. Roh *et al.*, Indocyanine green fluorescence lymphography during gastrectomy after initial endoscopic submucosal dissection for early gastric cancer. *Br. J. Surg.* **107**, 712–719 (2020).
27. C. Chi *et al.*, Use of indocyanine green for detecting the sentinel lymph node in breast cancer patients: From preclinical evaluation to clinical validation. *PLoS One* **8**, e83927 (2013).
28. T. Ishizawa *et al.*, Real-time identification of liver cancers by using indocyanine green fluorescent imaging. *Cancer* **115**, 2491–2504 (2009).
29. B. E. Schaafsma *et al.*, The clinical use of indocyanine green as a near-infrared fluorescent contrast agent for image-guided oncologic surgery. *J. Surg. Oncol.* **104**, 323–332 (2011).
30. R. A. Sheth *et al.*, Prospective trial with optical molecular imaging for percutaneous interventions in focal hepatic lesions. *Radiology* **274**, 917–926 (2015).

MEDICAL SCIENCES

www.manaraa.com